Reaction of (*S*)-BINAP with $H_4Ru_4(CO)_{12}$. The First Example of Face-Bridging BINAP Coordination and 100% Stereoselectivity in Formation of a Chiral Tetranuclear Cluster Framework

Sergey P. Tunik,*,† Tatiana S. Pilyugina,† Igor O. Koshevoy,† Stanislav I. Selivanov,† Matti Haukka,‡ and Tapani A. Pakkanen‡

Department of Chemistry, St. Petersburg University, Universitetskii pr., 26, St. Petersburg 198504, Russian Federation, and Department of Chemistry, University of Joensuu, P.O. Box 111, FIN-80101 Joensuu, Finland

Received November 10, 2003

The reaction of $H_4Ru_4(CO)_{12}$ with (*S*)-BINAP in the presence of Me_3NO affords the cluster $H_4Ru_4(CO)_{10}(\mu$-(*S*)-BINAP) (**2**) in good yield. Gentle heating of a benzene−ethanol solution of **2** results in the dissociation of CO and coordination of a naphthyl fragment of BINAP to give $H_4Ru_4(CO)_9(\mu_3$-(*S*)-BINAP) (**3**) with face-bridging coordination of the diphosphine ligand. The solid-state structures of both clusters have been determined by X-ray crystallography. Their structures in solution and some details of ligand sphere dynamics have been elucidated using 1D variable-temperature ^1H and ^{31}P NMR spectroscopy together with selective decoupling measurements and ^1H COSY and NOESY experiments. The difference ^1H nuclear Overhauser effect (NOE) spectra provide additional support for the structural models suggested by visualization of important intramolecular nonbonding contacts in the molecules under study. The metal frameworks in **2** and **3** are chiral, due to the chemical difference of the ruthenium atoms induced by asymmetry of their ligand environments. The chemical reactions, which result in the formation of **2** and **3**, display exceptional stereoselectivity to give a unique *S,S* configuration of the two ((*S*)-BINAP and cluster framework) stereogenic centers in the both compounds. The NMR and CD spectroscopic studies indicated that the *S,S* configuration observed in the solid state remains unchanged in solution. The cluster **3**, containing face-bridging BINAP, demonstrates exceptional thermal stability and does not undergo metal framework racemization up to 343 K.

Introduction

Asymmetric induction of a wide range of mononuclear transition-metal complexes containing the ligand 2,2′-bis(diphenylphosphino)-1,1′-binaphthyl (BINAP) in various catalytic reactions is well documented.[1−4] The degree of induction and, consequently, enantiomeric excess of the reaction products are dictated by the properties of the chiral pocket formed by BINAP in the coordination sphere of a catalyst, which in turn is determined by the ligand coordination mode and by location of the vacancies available for coordination of catalytic substrates. The chelating coordination of BINAP is a common structural motif for mononuclear complexes, and the corresponding coordination and catalytic chemistry has been studied in detail. Bonding of BINAP in transition-metal clusters may give rise, at least in principle, to both chelating and bridging coordination modes, making this chemistry more diverse and potentially providing other ways for the transfer of chiral induction in these complexes. It is worth noting that chiral induction in the BINAP-containing polynuclear complexes may be enhanced and modified by asymmetry of the other chiral elements, such as asymmetric metal frameworks, which are chiral due to the difference in ligand environment of each metal center.[5−8] These additional opportunities make the coordination chemistry of BINAP in transition-metal clusters especially interesting and promising from the viewpoint of directed chiral pocket design. This also means that investigation of the structure and dynamic properties of these compounds may shed light on the nature of chiral induction in related catalytic reactions. However, at present this chemistry has not received sufficient attention. Very few examples of synthetic and structural studies of BINAP-containing transition-metal clusters have been pub-

* To whom correspondence should be addressed. E-mail: stunik@chem.spbu.ru.
† St. Petersburg University.
‡ University of Joensuu.

(1) Noyori, R. *Asymmetric Catalysis in Organic Synthesis*; Wiley: New York, 1994.
(2) Noyori, R. In *Stereocontrolled Organic Synthesis*; Trost, B., Ed.; Blackwell: Oxford, U.K., 1994; p 1.
(3) Akutagawa, S. In *Asymmetric Synthesis by Ru-BINAP*; Scaros, M. G., Prunier, M. L., Eds.; Marcel Dekker: New York, 1995; p 135.
(4) Procter, G. *Asymmetric Synthesis*; Oxford University Press: Oxford, U.K., 1996.
(5) Bruce, M. I.; Nicholson, B. K.; Patrick, J. M.; White, A. H. *J. Organomet. Chem.* **1983**, *254*, 361−9.
(6) Collin, J.; Jossart, C.; Balavoine, G. *Organometallics* **1986**, *5*, 203−208.
(7) Deeming, A. J.; Stchedroff, M. J.; Whittaker, C.; Arce, A. J.; De Sanctis, Y.; Steed, J. W. *J. Chem. Soc., Dalton Trans.* **1999**, 3289.
(8) Tunik, S. P.; Koshevoy, I. O.; Poe, A. J.; Farrar, D. H.; Nordlander, E.; Haukka, M.; Pakkanen, T. A. *Dalton* **2003**, 2457.

10.1021/om034288n CCC: $27.50
Publication on Web 01/07/2004

lished.[9−14] It is interesting that even the limited number of complexes obtained demonstrated an unusual diversity of BINAP coordination modes to give chelate,[11,14] bridging,[9,12] and monodentate[11] bonding of the ligand to polynuclear metal frameworks.

The well-known catalytic activity of $H_4Ru_4(CO)_{12}$ and its derivatives in various organic reactions[15−21] makes this cluster very attractive for the investigation of its reactions with chiral ligands to obtain asymmetric catalysts with different and modifiable properties. A few synthetic and catalytic studies in this area have already been carried out,[22−25] including the synthesis of the cluster $H_4Ru_4(CO)_{10}$(1,1-BINAP) (**1**),[14] where the diphosphine occupies a chelating position at a ruthenium atom of the tetranuclear framework. However, extremely forcing conditions used in this synthesis (150 °C, 150 atm of H_2) and low product yield motivated us to reinvestigate this reaction. Two new compounds, $H_4Ru_4(CO)_{10}(\mu$-(*S*)-BINAP) (**2**) and $H_4Ru_4(CO)_9(\mu_3$-(*S*)-BINAP) (**3**), have been obtained under relatively mild conditions using a modified synthetic procedure. In the present paper we report the synthesis and X-ray structural characterization of **2** and **3** together with the NMR study of their solution structure and stereochemical nonrigidity of the hydride ligands. In both cases incorporation of BINAP into the coordination sphere of $H_4Ru_4(CO)_{12}$ demonstrated a unique (100%) stereoselectivity in formation of the chiral "*S*-Ru_4" framework, which is asymmetric due to different ligand environments at each Ru atom of the tetrahedral skeleton. The chiral framework configuration in **3** proved to be unexpectedly stable. It remains intact throughout a wide temperature range, which is indicative of the cluster potential in possible catalytic applications. Absolute configurations of chiral elements in **2** and **3** has been determined in the solid state by X-ray crystallography and confirmed in solution by multinuclear NMR and CD measurements.

Experimental Section

General Comments. The starting complex $H_4Ru_4(CO)_{12}$ was prepared according to the published procedure.[26] (*S*)-BINAP (Aldrich) and reagent grade solvents—dichloromethane, hexane, benzene, ethanol, and methanol (Vekton)—were dried over appropriate drying agents and distilled prior to use. All manipulations of the starting materials and reaction mixtures were carried out under an atmosphere of argon using standard Schlenk techniques. The products were purified by column chromatography on silica (5−40 mesh) in air. Fast atom bombardment (FAB+) mass spectra were obtained on a JEOL SX-102 instrument; 3-nitrobenzyl alcohol was used as a matrix and CsI as a calibrant. The observed isotopic distribution patterns fit completely to the calculated ones. The IR spectra were recorded on Nicolet 550 Magna FTIR and Specord M80 spectrometers. Microanalyses were carried out in the Analytical Laboratory of the University of Joensuu.

NMR Measurements. The ^{1}H, ^{13}C, and ^{31}P NMR spectra were recorded on Bruker DPX 300 and Bruker AM 500 spectrometers operating at the proton nominal frequency of 300 and 500 MHz. The chemical shifts were referenced to residual solvent resonances and external 85% H_3PO_4 in ^{1}H, ^{13}C, and ^{31}P spectra, respectively. All data were acquired, processed, and displayed using Bruker XWINNMR software and standard pulse-sequence library. The 2D COSY spectra were recorded using the magnitude mode, and NOESY data were acquired in the phase-sensitive mode at a mixing time of 0.5 s. The accuracy of the temperature measurements in the variable-temperature (VT) experiments was ±1.0 °C.

Synthesis of $H_4Ru_4(CO)_{10}(\mu_2$-(*S*)-BINAP) (2). $H_4Ru_4(CO)_{12}$ (102 mg, 0.137 mmol) and (*S*)-BINAP (86 mg, 0.138 mmol) were suspended in degassed benzene (12 cm^3) under an argon atmosphere, and a degassed solution of $Me_3NO{\cdot}2H_2O$ (32 mg, 0.288 mmol) in methanol (5 cm^3) was added dropwise with vigorous stirring. Addition of Me_3NO results in immediate formation of a transparent red solution.

A. A Schlenk tube containing the reaction mixture was placed into an oil bath (55 °C) and heated with stirring for 20−30 min. By this time the solution had darkened and a TLC spot test (eluant CH_2Cl_2−hexane (2/5 v/v)) showed the presence of two main products, **1** (orange band) and **2** (red-brown band). The solvents were then removed in vacuo. The remaining solid was dissolved in 1.5 cm^3 of dichloromethane and this solution diluted with 3 cm^3 of hexane, leaving some insoluble orange crystalline material. The solution was then purged (ca. 2 min) with CO and transferred onto a chromatographic column (2.5 × 10 cm). Careful separation of the sample (R_f parameters of **1** and **2** are very close to each other) using a CH_2Cl_2−hexane (2/5 v/v) mixture gave a bright orange band of $H_4Ru_4(CO)_{10}$-(1,1-(*S*)-BINAP) (**1**; 55 mg, 31%) and a wide red-brown band of $H_4Ru_4(CO)_{10}(\mu$-(*S*)-BINAP) (**2**; 105 mg, 59%).

B. The reaction mixture was left under argon at room temperature overnight, yielding a dark red solution and some amorphous precipitate. A TLC spot test (eluant CH_2Cl_2−hexane (2/5 v/v)) showed the presence of **1** and **2**. The solvents were removed in vacuo. The remaining solid was dissolved in 1.5 cm^3 of dichloromethane, and this solution was diluted with 3 cm^3 of hexane (leaving some insoluble orange crystalline material). The solution was purged (for ca. 2 min) with CO and transferred onto a chromatographic column (2.5 × 10 cm). Elution with a CH_2Cl_2−hexane mixture (2/5 v/v) gave a bright orange band of **1** (20 mg, 11%) and a wide red-brown band of **2** (128 mg, 71%).

Spectroscopic characteristics are as follows.

1. IR (ν(CO)/cm^{-1}; hexane): 2075 m, 2045 s, 2025 s, 2004 m, 1994 w, 1985 w, 1975 w. ^{1}H NMR (δ/ppm (J, Hz); $CDCl_3$, T = 253 K): hydride signals, −16.6 (s), −16.8 (dd, J(H−P) = 32.6 and 17.3), −17.1 (t, J(H−P) = 8.3), −17.7 (dd, J(H−P) =

(9) Derdau, V.; Laschat, S.; Dix, I.; Jones, P. G. *Organometallics* **1999**, *18*, 3859.
(10) Casado, M. A.; Perez-Torrente, J. J.; Ciriano, M. A.; Oro, L. A.; Orejon, A.; Claver, C. *Organometallics* **1999**, *18*, 3035.
(11) Deeming, A. J.; Stchedroff, M. *J. Chem. Soc., Dalton Trans.* **1998**, 3819.
(12) Deeming, A. J.; Speel, D. M.; Stchedroff, M. *Organometallics* **1997**, *16*, 6004.
(13) Prestopino, F.; Persson, R.; Monari, M.; Focci, N.; Nordlander, E. *Inorg. Chem. Commun.* **1998**, *1*, 302.
(14) Braga, D.; Matteoli, U.; Sabatino, P.; Scrivanti, A. *J. Chem. Soc., Dalton Trans.* **1995**, 419.
(15) Bianchi, M.; Menchi, G.; Francalanci, F.; Piacenti, F.; Matteoli, U.; Frediani, P.; Botteghi, C. *J. Organomet. Chem.* **1980**, *188*, 109.
(16) Doi, Y.; Tamura, S.; Koshizuka, K. *J. Mol. Catal.* **1983**, *19*, 213.
(17) Schmidt, G. F.; Reiner, J.; Suss-Fink, G. *J. Organomet. Chem.* **1988**, *355*, 379.
(18) Bhaduri, S.; Sharma, K.; Mukesh, D. *J. Chem. Soc., Dalton Trans.* **1992**, 77.
(19) Adams, R. D.; Falloon, S. B. *Organometallics* **1995**, *14*, 4594.
(20) Castiglioni, M.; Giordano, R.; Sappa, E. *J. Organomet. Chem.* **1995**, *491*, 111.
(21) Ellis, D. J.; Dyson, P. J.; Parker, D. G.; Welton, T. *J. Mol. Catal. A: Chem.* **1999**, *150*, 71.
(22) Homanen, P.; Persson, R.; Haukka, M.; Pakkanen, T. A.; Nordlander, E. *Organometallics* **2000**, *19*, 5568.
(23) Salvini, A.; Frediani, P.; Bianchi, M.; Piacenti, F.; Pistolesi, L.; Rosi, L. *J. Organomet. Chem.* **1999**, *582*, 218.
(24) Matteoli, U.; Beghetto, V.; Scrivanti, A. *J. Mol. Catal. A: Chem.* **1996**, *109*, 45.
(25) Scarpi, D.; Menchi, G.; Occhiato, E. G.; Guarna, A. *J. Mol. Catal. A: Chem.* **1996**, *110*, 129.
(26) Knox, S. A. R.; Koepke, J. W.; Andrews, M. A.; Kaesz, H. D. *J. Am. Chem. Soc.* **1975**, *97*, 3942.

30.7 and 19.2). These data fit completely the IR and ^{1}H NMR spectroscopic data obtained earlier for $H_4Ru_4(CO)_{10}$(1,1-(*S*)-BINAP).[14]

2. IR (ν(CO)/cm^{-1}; hexane): 2072 s, 2049 m, 2033 s, 2026 sh, 2010 m, 2003 w, 1989 w, 1980 w, 1966 w. ^{1}H NMR (δ/ppm (*J*, Hz); $CDCl_3$, *T* = 258 K): phenyl and naphthyl signals, 8.2−5.2, −16.5 (2H, d, *J*(H−P) = 11.7 and dd, *J*(H−P) = 23.5 and 11.5), −16.3 (d, *J*(H−P) = 32.3) −17.2 (dq, *J*(H−P) = 10.3, *J*(H−H) = ca. 2). ^{31}P{^{1}H} NMR (δ/ppm; $CDCl_3$, *T* = 283 K): 42.9, 28.4. FAB-MS (*m*/*z*): 1311 [M$^+$] (calcd 1311), [M$^+$ − *n*CO], *n* = 1−10. Anal. Calcd for $C_{54}H_{36}O_{10}P_2Ru_4$: C, 49.47; H, 2.77. Found: C, 49.46; H, 2.99.

Single crystals of **2** suitable for X-ray analysis were obtained by slow diffusion of hexane vapor into a $CH_3OH-CH_2Cl_2$ solution under an argon atmosphere.

Synthesis of $H_4Ru_4(CO)_9(\mu_3$-(*S*)-BINAP) (3). A 100 cm^3 Schlenk tube was charged with $H_4Ru_4(CO)_{10}(\mu_2$-(*S*)-BINAP) (92 mg, 0.07 mmol), benzene (20 cm^3), and absolute ethanol (15 cm^3). The resulting red solution was purged with argon for 3−5 min and evacuated. The Schlenk tube was then placed in an oil bath (80 °C) and stirred for 40 h. During this time evacuation was repeated periodically until a TLC spot test (eluant CH_2Cl_2−hexane (2/3 v/v)) showed complete consumption of the starting cluster. The TLC spot test also showed the presence of the new complex **3** along with trace amounts of **1**. The reaction mixture was reduced in volume in vacuo to ca. 15 cm^3 and diluted with degassed 2-propanol (10 cm^3). Further removal of the solvent, addition of octane (10 cm^3), and final reduction in volume to 10 cm^3 gave a red crystalline precipitate. The mixture was left for 30 min to complete precipitation. The pale mother liquor was decanted, and the remaining solid was successively washed with a degassed 2-propanol−heptane mixture (1/2 v/v; 5 cm^3) and heptane (2 × 5 cm^3) and dried in vacuo to give 72 mg (80%) of $H_4Ru_4(CO)_9(\mu_3$-(*S*)-BINAP) (**3**). IR (ν/cm^{-1}; hexane): 2070 w, 2060 s, 2040 s, 2009 s, 1997 m, 1970 w. ^{1}H NMR (δ/ppm (*J*, Hz); $CDCl_3$, 214 K): phenyl and naphthyl signals, 8.3−5.0, −15.3 (dm, ^2J(P−H) = 38.1), −15.7 (dd, ^2J(P−H) = 25.6 and 10.9), −16.5 (d, ^2J(P−H) = 14), −17.8 (br m). The last signal displays ^2J(P−H) = ca. 10 Hz at 210 K in CD_2Cl_2. ^{31}P{^{1}H} NMR (δ/ppm (*J*, Hz); $CDCl_3$, 293 K): 49.5 (d, 1P, *J*(P−P) = 2.8), 27.4 (d, 1P, *J*(P−P) = 2.8). FAB-MS (*m*/*z*): 1283 [M$^+$] (calcd 1283), [M$^+$ − *n*CO], *n* = 1−9. Anal. Calcd for $C_{53}H_{36}O_9P_2Ru_4$: C, 49.61; H, 2.83. Found: C, 49.20; H, 3.03.

Single crystals of **3** suitable for X-ray analysis were obtained by slow diffusion of methanol into a dichloromethane solution of **3** at room temperature.

X-ray Structure Determinations. The crystals were immersed in perfluoropolyether, mounted in a cryo loop, and measured at a temperature of 100 K or 120 K. The X-ray diffraction data were collected with a Nonius KappaCCD diffractometer using Mo Kα radiation (λ = 0.710 73 Å). The Denzo-Scalepack[27] program package was used for cell refinements and data reduction. All structures were solved by direct methods using the SHELXS-97 program and the WinGX graphical user interface.[28,29] A multiscan absorption correction based on equivalent reflections (XPREP in SHELXTL v. 6.12)[30] was applied to structure **2** (T_{min}/T_{max} = 0.123 72/0.169 17). Structural refinements were carried out with SHELXH-97[31] for **2** and with SHELXL-97[32] for **3**. Structure **3** contained a hexanemolecule in the asymmetric unit. Hexane carbons were refined with equal anisotropic displacement parameters. The structure of poorly diffracting **2** was solved in the chiral space group $P2_12_12_1$. The asymmetric unit consists of three independent $H_4Ru_4(CO)_{10}$(BINAP) molecules, due to the presence of two isomers. The ratio of the isomers is thus 2:1. Positions of hydrides were estimated by the XHYDEX[33] program. All other hydrogens were placed in idealized positions and constrained to ride on their parent atom. The crystallographic data are summarized in Table 1. Selected bond lengths and angles are shown in Table 2.

Table 1. Crystal Data for $H_4Ru_4(CO)_{10}$((*S*)-BINAP) (2) and $H_4Ru_4(CO)_9$((*S*)-BINAP)·C_6H_{14} (3)

	2	**3**
empirical formula	$C_{54}H_{36}O_{10}P_2Ru_4$	$C_{59}H_{50}O_9P_2Ru_4$
fw	1311.05	1369.21
temp (K)	100(2)	120(2)
λ (Å)	0.710 73	0.710 73
cryst syst	orthorhombic	orthorhombic
space group	$P2_12_12_1$	$P2_12_12_1$
a (Å)	14.0399(2)	13.5301(2)
b (Å)	22.1665(3)	19.7539(4)
c (Å)	47.2933(6)	20.7708(4)
V (Å^3)	14718.4(3)	5551.5(2)
Z	12	4
ρ_{calcd} (Mg/m^3)	1.775	1.638
μ(Mo Kα) (mm^{-1})	1.333	1.180
R1[a] ($I \geq 2\sigma$)	0.0320	0.0514
wR2[b] ($I \geq 2\sigma$)	0.0683	0.0866

[a] $R1 = \Sigma||F_o| - |F_c||/\Sigma|F_o|$. [b] $wR2 = [\Sigma[w(F_o^2 - F_c^2)^2]/\Sigma[w(F_o^2)^2]]^{1/2}$.

Results and Discussion

Syntheses and Solid-State Structures of 2 and 3. Reaction of $H_4Ru_4(CO)_{12}$ with (*S*)-BINAP in the presence of Me_3NO gives two isomers, **1** and **2**, of the $H_4Ru_4(CO)_{10}$(BINAP) stoichiometry in a very good (90%) total yield. Careful chromatographic separation of the reaction mixture affords both compounds in a pure state. It seems that the harsh conditions employed in the previously reported reaction of $H_4Ru_4(CO)_{12}$ and (*S*)-BINAP[14] prevented formation and isolation of **2**, which proved to be the major product in the synthesis described above. Single-crystal X-ray structural characterization of **1**[14] revealed that the cluster contains (*S*)-BINAP coordinated to a ruthenium atom in a chelating manner. In contrast, **2** displays a bridging coordination mode of the BINAP ligand, which spans an edge of the closed ruthenium tetrahedron. Gentle heating of **2** in a benzene/ethanol solution results in nearly quantitative elimination of CO and formation of $H_4Ru_4(CO)_9(\mu_3$-(*S*)-BINAP) (**3**), where the diphosphine occupies a face-bridging position over a ruthenium triangle. Coordination of BINAP to the third ruthenium atom in an η^2 mode occurs through an aromatic ring of the ligand naphthyl system. The solid-state structures of **2** and **3** have been determined using single-crystal X-ray diffraction; selected bond lengths and angles are given in Table 2, and molecular structures are shown in Figures 1 and 2, respectively.

Structure of 2. Three independent molecules have been found in the unit cell of **2**; two of them (**A** and **B**) are essentially similar and display only minor variations in bond lengths and angles. The third molecule (**C**) can be considered as a conformer of the **A**,**B** structure with

(27) Otwinowski, Z.; Minor, W. *Macromolecular Crystallography*; Methods in Enzymology 276; Carter, J. C. W., Sweet, R. M., Eds.; Academic Press: New York, 1997; Part A, p 307.
(28) Sheldrick, G. M. SHELXS97, Program for Crystal Structure Determination; University of Gottingen, Gottingen, Germany, 1997.
(29) Farrugia, L. J. *J. Appl. Crystallogr.* **1999**, *32*, 837.
(30) Sheldrick, G. M. SHELXTL Version 5.1; Bruker Analytical X-ray Systems, Madison, WI, 1998.
(31) Sheldrick, G. M. SHELXH-97; University of Gottingen, Gottingen, Germany, 1997.
(32) Sheldrick, G. M. SHELXL97, Program for Crystal Structure Refinement; University of Gottingen, Gottingen, Germany, 1997.
(33) Orpen, A. G.; XHYDEX. *J. Chem. Soc., Dalton Trans.* **1980**, 2509.

Table 2. Selected Bond Lengths (Å) and Angles (deg) for $H_4Ru_4(CO)_{10}$((*S*)-BINAP) (2) and $H_4Ru_4(CO)_9$((*S*)-BINAP) (3)

Bond Lengths

	2A	2C	3		2A	2C	3
C(1)−Ru(1)	1.844(11)	1.862(9)	1.881(8)	C(21)−C(29)	1.438(11)	1.441(11)	1.453(9)
C(2)−Ru(1)	1.878(10)	1.885(11)	1.870(8)	C(22)−C(23)	1.418(11)	1.435(11)	1.387(10)
C(3)−Ru(2)	1.917(12)	1.892(9)	1.885(9)	C(22)−P(1)	1.873(8)	1.851(8)	1.873(7)
C(4)−Ru(2)	1.896(9)	1.889(10)	1.888(10)	C(23)−C(24)	1.360(11)	1.337(11)	1.380(10)
C(5)−Ru(3)	1.924(11)	1.933(9)	1.933(9)	C(24)−C(30)	1.408(12)	1.430(11)	1.388(11)
C(6)−Ru(3)	1.915(11)	1.914(11)	1.887(8)	C(25)−C(26)	1.315(12)	1.372(12)	1.379(12)
C(7)−Ru(3)	1.880(9)	1.908(9)	1.875(8)	C(25)−C(30)	1.415(12)	1.430(11)	1.415(10)
C(8)−Ru(4)	1.890(10)	1.888(9)	1.849(8)	C(26)−C(27)	1.403(12)	1.393(12)	1.410(11)
C(9)−Ru(4)	1.895(9)	1.913(10)	1.879(10)	C(27)−C(28)	1.383(11)	1.364(11)	1.361(10)
C(10)−Ru(4)	1.941(10)	1.906(12)	-	C(28)−C(29)	1.419(11)	1.429(11)	1.416(10)
C(12)−C(13)	1.432(11)	1.389(12)	1.468(9)	C(29)−C(30)	1.424(12)	1.413(12	1.416(10)
C(12)−P(2)	1.830(8)	1.867(9)	1.834(8)	P(1)−Ru(1)	2.392(2)	2.370(2)	2.3652(19)
C(13)−C(14)	1.349(12)	1.358(11)	1.369(10)	P(2)−Ru(2)	2.353(2)	2.375(2)	2.3554(19)
C(14)−C(20)	1.406(12)	1.404(11)	1.413(11)	Ru(1)−Ru(3)	2.7935(9)	2.7523(9)	2.7548(8)
C(15)−C(16)	1.382(12)	1.378(12)	1.351(12)	Ru(1)−Ru(4)	2.9294(10)	2.9546(10)	2.9487(8)
C(15)−C(20)	1.428(11)	1.437(11)	1.420(11)	Ru(1)−Ru(2)	2.9765(10)	2.9639(10)	2.9617(9)
C(16)−C(17)	1.411(13)	1.376(13)	1.395(12)	Ru(2)−Ru(4)	2.9592(10)	2.9905(10)	3.0516(9)
C(17)−C(18)	1.344(12)	1.373(12)	1.379(11)	Ru(2)−Ru(3)	2.9733(9)	3.0196(9)	2.9530(9)
C(18)−C(19)	1.428(11)	1.421(11)	1.422(10)	Ru(3)−Ru(4)	2.7891(10)	2.7598(10)	2.7384(9)
C(19)−C(20)	1.415(12)	1.410(11)	1.400(10)	C(13)−Ru(4)			2.469(7)
C(21)−C(22)	1.393(11)	1.397(11)	1.403(10)				

Bond Angles

	2A	2C	3		2A	2C	3
C(37)−P(1)-Ru(1)	119.6(3)	121.2(3)	115.0(2)	C(5)−Ru(3)−Ru(4)	97.1(3)	96.8(3)	103.6(3)
C(31)−P(1)−Ru(1)	102.3(3)	117.1(3)	105.4(2)	C(7)−Ru(3)−Ru(1)	89.2(3)	92.7(3)	94.4(2)
C(22)−P(1)−Ru(1)	125.9(3)	103.7(3)	126.0(2)	C(6)−Ru(3)−Ru(1)	104.6(3)	100.3(2)	96.7(3)
C(49)−P(2)−Ru(2)	115.8(3)	115.9(3)	117.6(2)	C(5)−Ru(3)−Ru(1)	160.1(3)	161.4(3)	163.3(3)
C(43)−P(2)−Ru(2)	113.9(3)	105.8(3)	118.3(2)	Ru(4)−Ru(3)−Ru(1)	63.30(2)	64.83(3)	64.93(2)
C(12)−P(2)−Ru(2)	111.0(3)	126.4(3)	104.6(2)	C(7)−Ru(3)−Ru(2)	151.1(3)	152.3(3)	145.5(2)
P(1)−Ru(1)−Ru(3)	176.06(7)	166.53(6)	174.77(6)	C(6)−Ru(3)−Ru(2)	95.7(3)	100.8(2)	111.2(2)
P(1)−Ru(1)−Ru(4)	125.08(7)	119.89(7)	118.00(5)	C(5)−Ru(3)−Ru(2)	113.4(3)	108.7(3)	102.3(3)
Ru(3)−Ru(1)−Ru(4)	58.28(2)	57.71(2)	57.27(2)	Ru(4)−Ru(3)−Ru(2)	61.70(2)	62.13(2)	64.72(2)
P(1)−Ru(1)−Ru(2)	117.21(6)	103.21(6)	118.62(5)	Ru(1)−Ru(3)−Ru(2)	62.05(2)	61.59(2)	62.40(2)
Ru(3)−Ru(1)−Ru(2)	61.94(2)	63.65(2)	62.08(2)	C(8)−Ru(4)−Ru(3)	89.3(3)	88.7(3)	88.7(3)
Ru(4)−Ru(1)−Ru(2)	60.13(2)	60.70(2)	62.17(2)	C(9)−Ru(4)−Ru(3)	78.2(3)	81.0(3)	104.5(3)
C(4)−Ru(2)−P(2)	97.7(3)	97.0(3)	98.3(3)	C(10)−Ru(4)−Ru(3)	175.7(3)	173.8(3)	-
C(3)−Ru(2)−P(2)	95.2(3)	86.1(3)	97.4(2)	C(8)−Ru(4)−Ru(1)	143.8(3)	140.4(3)	146.5(3)
C(4)−Ru(2)−Ru(4)	99.8(3)	144.5(3)	103.8(3)	C(9)−Ru(4)−Ru(1)	93.6(3)	100.2(3)	98.5(2)
C(3)−Ru(2)−Ru(4)	147.0(3)	100.5(3)	158.9(3)	C(10)−Ru(4)−Ru(1)	119.6(3)	119.0(3)	
P(2)−Ru(2)−Ru(4)	111.49(6)	112.76(6)	90.14(5)	Ru(3)−Ru(4)−Ru(1)	58.42(2)	57.46(2)	57.80(2)
C(4)−Ru(2)−Ru(3)	102.9(3)	93.3(3)	100.2(3)	C(8)−Ru(4)−Ru(2)	91.1(3)	88.0(3)	106.0(3)
C(3)−Ru(2)−Ru(3)	92.0(2)	100.9(3)	112.8(2)	C(9)−Ru(4)−Ru(2)	139.8(3)	144.1(3)	157.1(3)
P(2)−Ru(2)−Ru(3)	157.42(6)	166.33(7)	142.87(6)	C(10)−Ru(4)−Ru(2)	120.7(3)	120.3(3)	
Ru(4)−Ru(2)−Ru(3)	56.09(2)	54.67(2)	54.23(2)	Ru(3)−Ru(4)−Ru(2)	62.21(2)	63.20(2)	61.05(2)
C(4)−Ru(2)−Ru(1)	155.5(3)	90.8(3)	154.9(3)	Ru(1)−Ru(4)−Ru(2)	60.72(2)	59.80(2)	59.12(2)
C(3)−Ru(2)−Ru(1)	97.8(3)	154.0(3)	100.5(3)	C(13)−Ru(4)−Ru(1)			104.27(16)
P(2)−Ru(2)−Ru(1)	101.75(6)	115.89(6)	99.47(5)	C(13)−C(14)−C(20)	120.3(9)	119.6(8)	120.8(7)
Ru(4)−Ru(2)−Ru(1)	59.14(2)	59.50(2)	58.71(2)	C(14)−C(13)−C(12)	122.3(8)	123.0(8)	120.6(7)
Ru(3)−Ru(2)−Ru(1)	56.01(2)	54.76(2)	55.52(2)	C(14)−C(13)−Ru(4)			81.4(4)
C(7)−Ru(3)−C(6)	94.6(4)	93.6(4)	95.8(4)	C(12)−C(13)−Ru(4)			104.5(4)
C(7)−Ru(3)−C(5)	92.5(4)	92.8(4)	96.1(4)	C(11)−C(12)−C(13)	118.7(8)	119.2(8)	118.7(7)
C(6)−Ru(3)−C(5)	95.0(4)	97.1(4)	95.0(4)	C(11)−C(12)−P(2)	128.2(6)	122.6(7)	128.7(5)
C(7)−Ru(3)−Ru(4)	104.1(3)	98.9(3)	82.8(2)	C(13)−C(12)−P(2)	113.0(6)	117.8(6)	111.6(6)
C(6)−Ru(3)−Ru(4)	157.2(3)	160.9(2)	161.3(3)				

a different orientation of the BINAP binaphthyl fragment relative to the Ru(1)Ru(2)Ru(4) face (see Figure 1). In the **A**,**B** structural pattern one of the naphthyl moieties is brought to close proximity to the metal triangle due to the particular mode of phosphorus atom coordination to the Ru(1)−Ru(2) edge. We believe that this coordination mode is dictated by a weak but important interaction (so-called dihydrogen bonding[34−37]) of a hydride ligand with the protons of the adjacent naphthyl moiety. As shown below by nuclear Overhauser effect (NOE) NMR measurements, the **A**,**B** conformation of **2** dominates in solution, and we believe that the presence of the **C** conformer in the crystal cell is a result of lattice packing effects. Because of this, essential structural features of the **A**,**B** conformer only will be discussed here in detail. The molecule consists of a ruthenium tetrahedron surrounded by 10 terminal COs, 4 bridging hydrides, and (*S*)-BINAP coordinated in the bridging position between Ru(1) and Ru(2). The electron count for **2** gives 60 electrons, which fits

(34) Richardson, T. B.; Koetzle, T. F.; Crabtree, R. H. *Inorg. Chim. Acta* **1996**, *250*, 69.
(35) Custelcean, R.; Jackson, J. E. *Chem. Rev.* **2001**, *101*, 1963.
(36) Xu, W.; Lough, A. J.; Morris, R. H. *Can. J. Chem.* **1997**, *75*, 475.
(37) Abramov, Y. A.; Brummer, L.; Klooster, W. T.; Bullock, R. M. *Inorg. Chem.* **1998**, *37*, 6317.

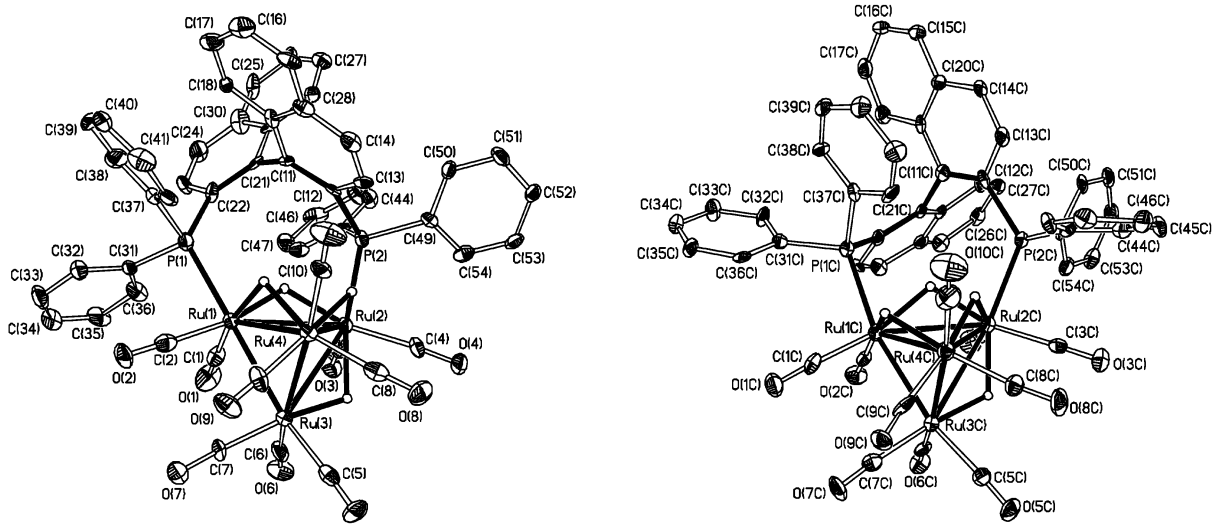

Figure 1. ORTEP plot of the molecular structure of $H_4Ru_4(CO)_{10}(\mu_2$-BINAP) (**2**). Thermal ellipsoids are drawn at the 50% level.

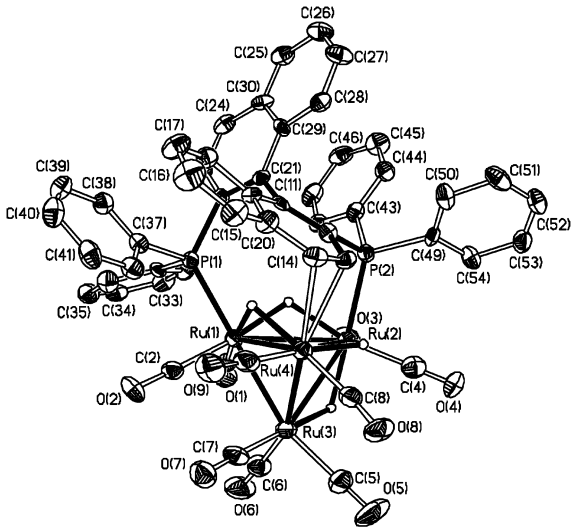

Figure 2. ORTEP plot of the molecular structure of $H_4Ru_4(CO)_9(\mu_3$-BINAP) (**3**). Thermal ellipsoids are drawn at the 50% level.

precisely with a closed configuration of the tetraruthenium core. Three of the bridging hydrides, H(01), H(02), and H(04), symmetrically surround the Ru(1)Ru(2)-Ru(4) triangle to occupy cis positions with respect to the phosphorus atoms of BINAP, whereas H(03) bridges the Ru(2)−Ru(3) edge in the position trans to P(2). This configuration of the hydride ligands is evidently a potential sink for the clusters of this sort, as the same ligand arrangement has been found in the other $H_4Ru_4(CO)_{10}(\mu$-PP) clusters[22,38,39] containing various diphosphines. The disposition of the four hydride bridges and two phosphorus atoms around the ruthenium tetrahedron makes it asymmetric (chiral), and all three molecules presented in the unit cell display identical stereoconfigurations of the metal framework. The geometry of the ruthenium tetrahedron is highly asymmetric as well. The four Ru−Ru bonds spanned by the hydride ligands are substantially longer (l_{av} = 2.9596 Å) compared to the other metal−metal distances (l_{av} = 2.7913 Å). This trend is typical for the diphosphine-substituted $H_4Ru_4(CO)_{12}$ derivatives, and a very similar elongation of the Ru−Ru bonds bridged by the hydride ligands was observed in the other $H_4Ru_4(CO)_{10}(\mu$-PP) clusters.[22,38,39] Bridging coordination of the diphosphine gives an eight-membered ligand containing the dimetallacycle, where the conformation of the BINAP backbone is substantially distorted compared to that of the free ligand. This distortion stems from the disparity between the ligand bite angle and available vacancies at adjacent ruthenium atoms and causes a strain in this cyclic molecular fragment because of the BINAP backbone rigidity. This strain is partially relieved through asymmetric coordination of the ligand: for example, the P(1)−Ru(1)−Ru(2) and P(2)−Ru(2)−Ru(1) angles in **2** are 117.2 and 101.8°, respectively. In the other $H_4Ru_4(CO)_{10}(\mu$-PP) clusters where diphosphines (dppm,[40] dppe,[39] and dppp[40]) form five-, six-, and seven-membered dimetallacycles containing relatively flexible hydrocarbon backbones, the angular distortions are substantially lower and variations in P−Ru−Ru bonding angles around the phosphorus atoms are at most 4.5° ($H_4Ru_4(CO)_{10}(\mu$-dppe)). It is interesting that two other compounds containing bridging BINAP, ((3,3-dimethylbutyne)(μ-(*R*)-BINAP)$Co_2(CO)_4$[9] and $Ru_3(\mu$-OH)$_2(CO)_8(\mu$-(*R*)-BINAP)[12]) display substantially different structural behavior: in the dicobalt complex the Co−Co−P angles equal 100.8 and 117.0°, whereas coordination of BINAP in the triruthenium cluster is essentially symmetric to give nearly equal P−Ru−Ru angles, 109.9 and 110.8°. Metal−metal bond distances in these complexes, 2.501 and 3.031 Å, respectively, may control the coordination geometry and related strain of the ligand bonding. However, the Ru(1)−Ru(2) bond length in **2** (2.9765(10) Å) is closer to the value in the trinuclear ruthenium

(38) Bruce, M. I.; Horn, E.; Bin Shawkataly, O.; Snow, M. R.; Tiekink, E. R. T.; Williams, M. L. *J. Organomet. Chem.* **1986**, *316*, 187.

(39) Churchill, M. A.; Lashewicz, R. A.; Shapley, J. R.; Richter, S. I. *Inorg. Chem.* **1980**, *19*, 1277.

(40) Puga, J.; Arce, A.; Braga, D.; Centritto, N.; Grepioni, F.; Castillo, R.; Ascanio, J. *Inorg. Chem.* **1987**, *26*, 867.

cluster, whereas the distortions observed resemble those in the dicobalt complex. These observations suggest that the asymmetry of bridging BINAP coordination cannot be completely assigned to the effect of different metal−metal distances spanned by the diphosphine, and the disparity between the ligand bite angle and the geometry of coordination vacancies at the corresponding ruthenium atoms seems to play a key role in the asymmetric coordination of BINAP in **2**.

The positions of 10 terminal CO ligands in **2** are very similar to those found in the other $H_4Ru_4(CO)_{10}(\mu$-PP) clusters.[22,38−40] Three CO ligands are bonded to unsubstituted Ru(3) and Ru(4), and two CO groups together with the phosphorus atoms of BINAP are bonded to Ru(1) and Ru(2). The Ru−C and C−O distances for the carbonyl ligands are also typical for these complexes and do not display any irregularities compared to analogous tetraruthenium clusters.[22,38−40] However, insertion of the sterically demanding BINAP into the coordination sphere of **2** results in rather short nonbonding contacts of C(10)O with C(13) and C(14) atoms of the naphthyl fragment: 3.305, 3.402, 3.488, and 3.160 Å, respectively. This interaction, in turn, bends the carbonyl ligand out of the Ru(1)Ru(2)Ru(4) triangle to increase the Ru(2)−Ru(4)−C(10) and Ru(1)−Ru(4)−C(10) angles up to 119.6 and 120.6°, respectively: cf. the average Ru−Ru−C cis angle (95.3(7.9)°) for the other carbonyl groups in **2**. This strain gives rise to easily predictable chemical consequences, which consist of labilization of C(10)O and spontaneous substitution of this ligand by the adjacent naphthyl group of BINAP to give **3**. As the reaction slowly occurs at room temperature, gentle heating of a benzene−ethanol solution of **2** is a convenient synthetic route to **3**.

Figure 2 shows the ORTEP plot of **3**. This is the first example of BINAP face-bridging coordination, where a naphthyl fragment serves as an additional two-electron-donor functionality. In an earlier study[11] it was shown that refluxing the $Os_3(CO)_{12}$ and (*R*)-BINAP mixture in octane eventually forces ortho metalation of a BINAP phenyl ring to give a face-bridging triosmium hydride cluster, which, however, differs substantially from the structural pattern shown in Figure 2. Coordination of the naphthyl fragments through a pseudo "double bond" of the aromatic system is well-known in organometallic chemistry, including a few examples of ruthenium and palladium BINAP complexes with the binaphthyl moiety coordination to the metal centers.[41−45] In the ruthenium complexes[41−45] BINAP donates an additional electron pair from a naphthyl fragment to relieve electronic unsaturation of the metal atom to form a stable 18-electron species. Geometry of the metal orbitals available for the interaction with the naphthyl fragment in these *mononuclear* complexes evidently dictates involvement of the $C_1−C_2$ bond in the coordination to the ruthenium center. In contrast, geometrical requirements in **3** result in coordination of the $C_3−C_4$ (C(13)−C(14)) bond to give the structure shown in Figure 2. This molecule consists of a closed ruthenium tetrahedron, in agreement with the 60-electron count, provided that the naphthyl group donates an electron pair to the Ru(4) atom. The position of the BINAP phosphorus atoms and four bridging hydride ligands around the tetrahedron is completely analogous to that found in **2**. Similarly to **2**, the four longest Ru−Ru bonds are spanned by hydrides; the average difference between two nonbridged (short) and hydride-bridged (long) bonds is about 0.2 Å. The loss of the C(10)O ligand did not result in a rearrangement of the other nine carbonyls, as they were found in their regular positions: two at each phosphorus-substituted Ru atom, two at the naphthyl-bonded Ru(4), and three at the unsubstituted Ru(3) atom. The average bond lengths for these carbonyl groups, $(Ru−C)_{av} = 1.883$ Å and $(C−O)_{av} = 1.445$ Å, are in very good agreement with the values found for the corresponding ligands in **2**. Coordination of the naphthyl fragment in **3** does not substantially affect the structural parameters of the aromatic system. Both naphthyl fragments remain nearly planar, and the bond lengths in the coordinated six-membered ring are only slightly elongated: $(C−C)_{av} = 1.414$ Å (cf. 1.408 Å for the corresponding noncoordinated naphthyl group in **2**). The coordinated C(13)−C(14) bond in **3** is even shortened compared to the same bond length in **2**. These observations point to an effective but complicated mechanism to dissipate the excitation inside the conjugated aromatic system caused by its bonding to a metal atom. As pointed out above, three bridging hydrides in **2** form a nearly symmetric "crown" around the Ru(1)Ru(2)-Ru(4) triangle, whereas coordination of the naphthyl group to Ru(4) in **3** results in folding of H(04) out of the plane to form a 174.5° angle between the ruthenium triangle and the Ru(2)H(04)Ru(4) bridge: cf. 120.3° revealed in **2**. The H(01) and H(02) hydride bridges keep an undistorted configuration, with the corresponding angles equal to 117.4 and 121.9°, respectively. Similarly to **2**, coordination of the BINAP phosphorus atoms in **3** is highly asymmetric, as shown by the angular parameters of this molecule: P(1)−Ru(1)−Ru(2) and P(2)−Ru(2)−Ru(1) are 118.6 and 99.5°, and Ru(1)−P(1) and Ru(2)−P(2) are 2.392(2) Å and 2.353(2) Å, respectively. The different ligand environment at each ruthenium atom makes the "Ru_4" tetrahedron chiral, and the asymmetry of the cluster framework found in the solid state remains unchanged in solution, which has been confirmed by a combination of NMR and circular dichroism (CD) measurements and will be discussed below.

Solution Structures of 2 and 3. The idealized structure of "$Ru_4(CO)_x$" ($x = 9$, 10) fragment in both clusters is not asymmetric because of a mirror plane through Ru(3), Ru(4), and the center of the Ru(1)−Ru(2) bond. Although insertion of the asymmetric diphosphine into this structural pattern makes the phosphorus atoms and the phosphorus-bound ruthenium atoms diastereotopic, the carbonyl environment and "$Ru_4(\mu$-PP)$(CO)_x$" fragment are still achiral. Therefore, in the following discussion we will focus on the structure and dynamic behavior of the "$H_4Ru_4(\mu$-PP)" fragment, since its stereochemistry is of crucial importance for the asymmetry of the molecules as a whole. Most of the

(41) Pathak, D. D.; Adams, H.; Bailey, N. A.; King, P. J.; White, C. *J. Organomet. Chem.* **1994**, *479*, 237.
(42) Kocovsky, V.; Vyskocil, S.; Cisarova, I.; Sejbal, V.; Tislerova, I.; Smrcina, M.; Lloyd-Jones, G. C.; Stephen, S. C.; Butts, C. P.; Murray, M.; Langer, V. *J. Am. Chem. Soc.* **1999**, *121*, 7714.
(43) Geldbach, T. J.; Pregosin, P. S.; Albinati, A. *Organometallics* **2003**, *22*, 1443.
(44) den Reijer, C. J.; Dotta, P.; Pregosin, P. S.; Albinati, A. *Can. J. Chem.* **2001**, *79*, 693.
(45) Cyr, P. W.; Rettig, S. J.; Patrick, B. O.; James, B. R. *Organometallics* **2002**, *21*, 4672.

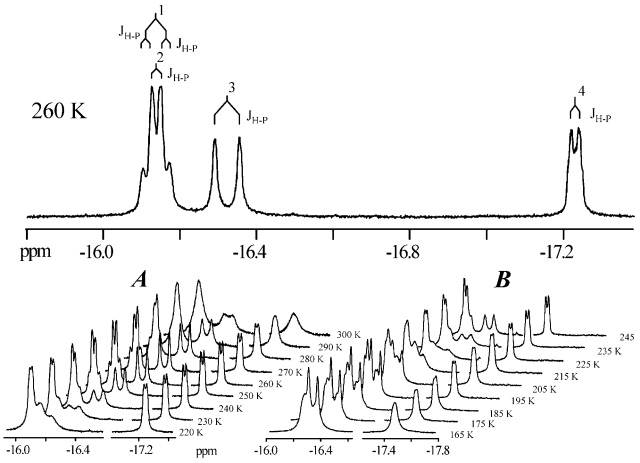

Figure 3. 500 MHz variable-temperature ^{1}H NMR spectra of **2** in the hydride region: (*A*) in $CDCl_3$; (*B*) in CD_2Cl_2. The spectrum recorded at 260 K is shown separately along with a schematic assignment of the hydride resonances.

NMR spectroscopic data obtained are available as Supporting Information; the numbers of the corresponding figures bear an "S" prefix. Only some indicative spectra related to the discussion are given in the main body of the text.

Cluster 2. The proton NMR measurements showed that at room temperature the molecule is stereochemically nonrigid. The signals of four hydrides (Figure 3) and the resonances of two inequivalent phosphorus atoms in the ^{31}P NMR spectrum are substantially broadened. This is evidently a result of intramolecular hydride exchange that has also been verified by ^{1}H NOESY measurements (Figure S1A), which showed scrambling of all hydrides between four available bridging positions. However, the dynamic process is frozen at 258 K, where one can observe a few fairly narrow resonances of inequivalent hydrides between −16.0 and −17.3 ppm in the proton NMR spectrum (Figure 3). It is worth noting that the NOESY spectrum (Figure S1B, 258 K) displays very weak exchange (positive) cross-peaks along with weak NOE (negative) signals. The weak exchange signals point to the slow rate of the hydride dynamics, whereas the NOE responses show the ability of the routine to detect the presence of adjacent hydrides.

The lowest field resonance, which looks like a slightly distorted quartet of double intensity, is in fact a combination of two overlapped signals (d and dd, as shown in Figure 3), distinguished by selective ^{1}H{^{31}P} and ^{31}P{^{1}H} decoupling measurements together with ^{1}H COSY experiments (Figure S2). The NMR data mentioned above also made it possible to construct a detailed diagram of two-bond ^{1}H−^{31}P and ^{1}H−^{1}H spin−spin couplings, shown in Chart 1, which allows complete assignment of the hydride signals schematically represented in the upper part of Figure 3. On the basis of this diagram, the low-field signal (49.5 ppm) in the ^{31}P spectrum of **2** coupled to three bridging hydrides should be associated with P(2), whereas the high-field resonance (27.4 ppm), which interacts with only two hydride ligands, should be associated with P(1). Of the four hydride resonances, three signals are coupled to a unique phosphorus nucleus, either P(1) or P(2), and only one displays coupling to both. These observations are

Chart 1. Diagrams of Spin−Spin Couplings in 2 and 3

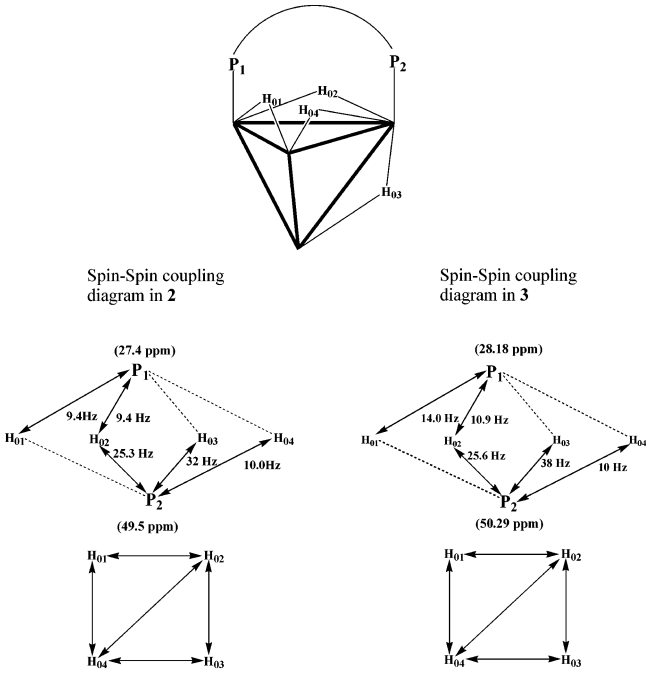

in complete agreement with the structure of the "$H_4Ru_4(\mu$-PP)" pattern found in the solid state, where H(03), H(04), and H(01) hydrides are in the vicinity of P(2) and P(1), respectively, and the "Ru(1)−Ru(2)" bridging position of H(02) allows two-bond coupling of this hydride to both phosphorus nuclei. Additionally, coupling of H(03) to P(2) shows the highest ^2J(P−H) value (32 Hz), which is consistent with the trans position of the intervening nuclei about Ru(2).

The other P−H coupling constants are about 10 Hz, except for ^2J(P(2)−H(02)), which is more than 2 times larger (25 Hz) than that of this hydride to P(1). This could be explained in terms of the H(02) semibridging position on the Ru(1)−Ru(2) edge. On the basis of the data obtained, it is hardly possible to ascribe this effect either to angular dependence of the two-bond coupling or to a difference in the H(02) to Ru(1) and Ru(2) distances. However, the asymmetry of the hydride bridging coordination with respect to the phosphorus atoms is clearly evident. The ^{1}H COSY spectrum in the hydride area together with selective ^{1}H{^{1}H} decoupling experiments showed all possible pairwise interactions between the hydrides (^2J(H−H) equal to ca. 2 Hz each), except that of H(01)−H(03). The latter observation is completely in line with the remote disposition of these two ligands on the tetraruthenium framework, in contrast to the other pairs of hydrides. The results of the proton NMR studies given above clearly point to an asymmetric location of the hydrides around the ruthenium tetrahedron and indicate that the structure of the "H_4Ru_4(PP)" fragment found in the solid state remains unchanged in solution at the low-temperature limit. It has to be mentioned that at temperatures below 258 K the signals of hydrides start to broaden (Figure 3), which is an indication of a dynamic process that affects the form of the lines observed in the temperature range 165−250 K. One of the possibilities is exchange between two forms of the molecule: for example, for the **A**,**B** ↔ **C** conformers found in the solid state. This suggestion

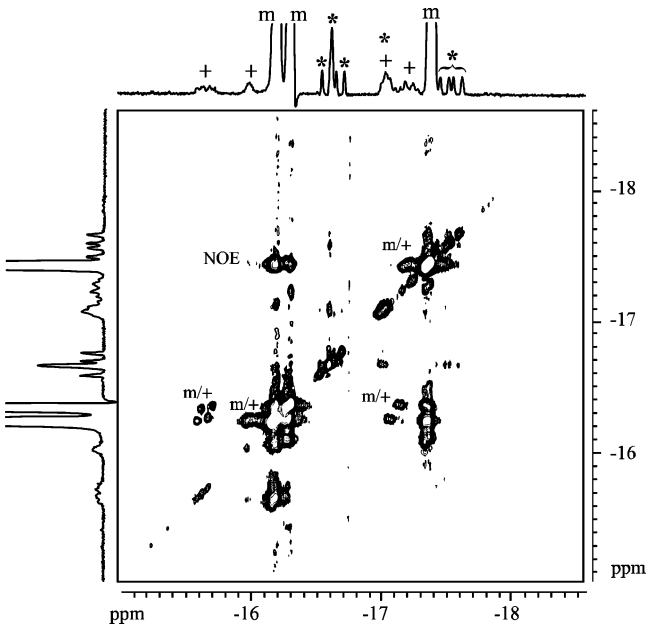

Figure 4. 300 MHz ^{1}H EXSY spectrum of **2** (in CD_2Cl_2, 193 K). 1D projections of the spectrum are enlarged 12 times to clearly show the signals of minor form of **2**, marked with a "+" symbol; "m" denotes the multiplets of the major form. The signals of an admixture are marked with asterisks. Major/minor form exchange cross-peaks are denoted "m/+".

is supported by the low-temperature ^{1}H NOESY spectrum of this system recorded at 183 K.

The spectrum clearly demonstrates the presence of another minor form of the cluster, which accounts for about 5% of the total amount under these conditions. Four cross-peaks (m/+) between the signals of major and minor forms clearly point to the presence of the exchange between these species at 183 K. The exchange is evidently responsible for the low-temperature broadening of the well-resolved signals observed in the spectrum recorded at 258 K (Figure 3). Thus, this spectrum represents averaged spectroscopic properties of the major and minor forms of **2** in solution. The essential feature of this spectrum consists of frozen intramolecular scrambling of the hydrides with simultaneous fast exchange between two species. These observations point to a very low kinetic barrier of the species interconversion, which is consistent with the exchange between structurally similar **A**,**B** and **C** conformers. It is worthwhile to stress at this point that the hydride to phosphorus and hydride to hydride spin−spin couplings in both conformers are essentially similar and the difference in binaphthyl moiety orientation in **A**,**B** and **C** does not affect the conclusions about the structure of the "H_4Ru_4(PP)" fragment drawn above. The low content of the minor form together with the poor solubility of the complex and high viscosity of the solution at 183 K prevented full characterization of this species. Nevertheless, the general structure of the signals observed in the hydride region points to the similarity of the hydride environment in both exchanging clusters and agrees well with assignment of these species to the pair of **A**,**B** and **C** conformers. The spectrum shown in Figure 4 also displays the cross-peaks between the signals of the major form, marked "NOE". We assign these cross-peaks to NOE enhancement due to the following reasons. First of all, there are no physical reasons for acceleration of the intramolecular hydride scrambling (which was nearly completely frozen at 258 K) with the decrease of temperature. Second, the NOE enhancements between "averaged" hydride signals of two forms were observed in the NOESY spectrum at 258 K (Figure S1B) as a few weak negative signals. The emergence of the positive NOE responses for the major form at 183 K can be explained by the well-known inversion of the NOE effect sign at the $\omega_0\tau_c = 1.12$ point while the temperature decreases (ω_0 is the Larmor frequency and τ_c is the correlation time of diffusion motion). The change of the NOE signal sign is also in line with the anisotropy of the overall diffusive motion for highly asymmetric molecules such as the cluster **2**.

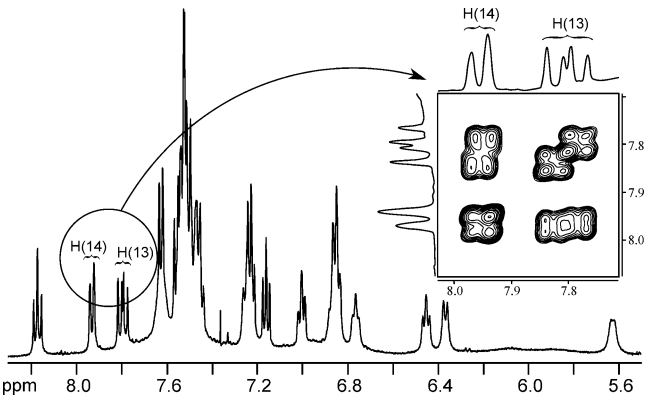

Figure 5. ^{1}H NMR spectrum of **2** in the aromatic region (in CD_2Cl_2, 260 K). The inset shows a part of the ^{1}H−^{1}H COSY spectrum related to H(13) and H(14) proton signals.

To assign the dominating form to one of the structural patterns observed in the solid state, it is important to find out an essential difference in these structures, which may allow discrimination of two structural hypotheses. It has been mentioned above that the **A**,**B** and **C** conformers differ in the distance between Ru(1)Ru(2)Ru(4) triangle and adjacent naphthyl moiety of BINAP. In particular, the close proximity of the metal triangle and the naphthyl moiety in the **A**,**B** conformer results in short contacts (2.34 Å) between the H(04) hydride and the H(13) proton. None of the binaphthyl protons in the conformer **C** display a similar short nonbonding distance to the hydride ligands. It is evident that ^{1}H difference nuclear Overhauser effect (NOE) measurements, which are highly sensitive to the distance between the intervening nuclei, can serve as a tool to distinguish the structures under question. The key point in the NOE study was unambiguous assignment of the protons in the naphthyl fragments, which has been made on the basis of ^{1}H−^{1}H COSY experiments (193 and 258 K, Figures S3 and S4) and selective ^{1}H{^{31}P} decoupling measurements. It is also worth noting that analysis of the low-temperature ^{1}H−^{1}H COSY spectrum in the aromatic area also points to the dominance of one major form of **2** in solution. It has been found that the dd signal at 7.78 ppm can be unambiguously assigned to H(13) because of its coupling both to P(2) and to only one (H(14)) proton (7.92 ppm) of the naphthyl fragment (Figure 5). This spectroscopic pattern can be generated by the interaction of H(13), H(14), and P(2) only, and no other protons in the BINAP bridge match this particular feature.

Chart 2. Schematic Structure and Diagram of Nonbonding Contacts in 2 and 3

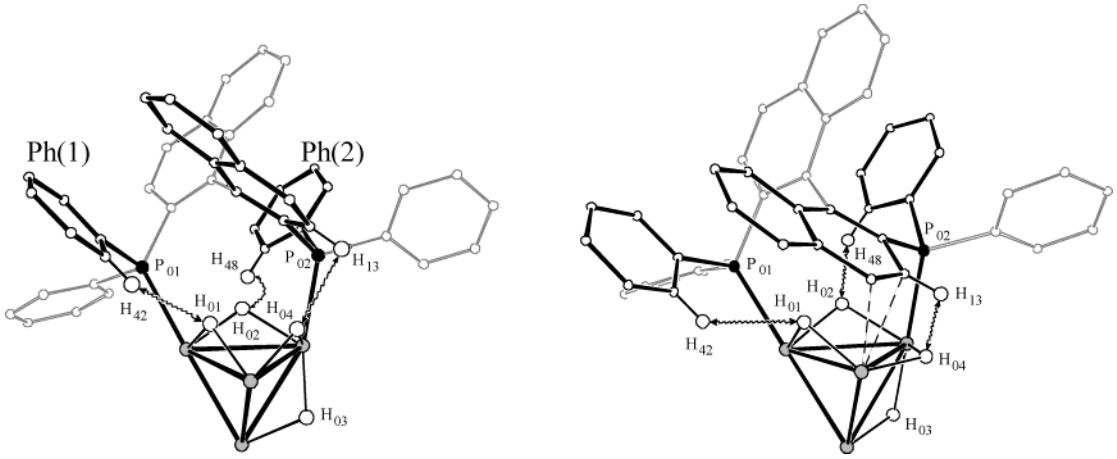

The NOE measurements (258 K, Figure S5) show that it is the **A**,**B** conformer that dominates in solution under these conditions. In accordance with the remote location of the H(03) hydride with respect to the BINAP aromatic protons, no related signals have been found in the corresponding NOE difference spectrum. In contrast, the other three hydrides display strong connectivities with the protons of the binaphthyl fragment and phenyl rings of BINAP. Irradiation of the H(04) hydride resonance led to NOE enhancement of the proton (dd) signal at 7.78 ppm, which has been assigned to H(13), and the emergence of the NOE difference signal points to the close proximity of these two nuclei in solution, as was found in the solid state. It is worth noting at this point that *none* of the hydrides in the structural pattern **C** display short (less than 3.0 Å) nonbonding contacts with the naphthyl protons. The shortest distances are about 4.2 Å, which is far beyond the limiting value expectable for a nonzero NOE response. These observations indicate the proximity of the naphthyl fragment to the ruthenium tetrahedron in the major form of **2** presented in solution at this temperature. This is completely compatible with the dominance of the **A**,**B** conformer in solution under these conditions. The solid-state structure of the **A**,**B** conformer also displays short intramolecular contacts of H(01) with H(42) (2.32 Å) and of H(02) with H(48) (2.15 Å) (see Chart 2). These contacts most likely account for the signals in the NOE spectrum generated by irradiation of H(01)/H(02) frequencies, separate irradiations of which are impossible due to nearly identical positions of the hydride resonances.

These NOE responses (multiplet at 7.25 ppm and two broadened signals at 5.8 and 7.8 ppm) can be assigned to ortho phenyl protons on the basis of their connectivities observed in the ^{1}H COSY spectrum (Figures S3 and S4) and their couplings to P(1) and P(2). Broadening of the resonances at 5.8 and 7.8 ppm is evidently a result of hindered rotation of the corresponding phenyl ring about the phosphorus−carbon bond, because both signals narrow down to well-resolved multiplets at lower temperature. A similar hindered rotation of the two phenyl rings in bridging BINAP has been found earlier in $Ru_3(CO)_8(\mu\text{-}OH)_2(\mu\text{-}(R)\text{-BINAP})$.[12] The authors assigned the hindrances to parallel alignment of the corresponding naphthyl and phenyl fragments, which is also observed in **2** for the Ph(1) and Ph(2) rings (see Chart 2). The phenyl ring rotation in this case may only occur through a transient state with a perpendicular orientation of these fragments, which results in emergence of a potential barrier for this rotation. In the triruthenium cluster symmetric coordination of BINAP made the phenyl rings and the corresponding barriers equivalent. In the cluster **2** asymmetric coordination of the phosphorus atoms of the diphosphine together with the interaction of the ortho protons of Ph(1) and Ph(2) rings with H(01) and H(02) makes the corresponding barriers different, which results in different dynamic behavior of the phenyl moieties.

Thus, the NMR data obtained for **2** showed that below 258 K the location of the hydride ligands around the tetraruthenium skeleton matches well the structural pattern found in the solid state. The NOE measurements provided clear indication that the **A**,**B** conformation dominates in solution in the temperature range studied. The **A**,**B** and **C** conformers do not display substantial differences in structural parameters (bond lengths and angles, Table 2) normally used in discriminative analysis of molecular conformations. The variations observed can hardly discriminate the energy of **A**,**B** and **C** to provide domination of the former structure in solution. However, one can notice that these two forms of **2** are distinguished by left and right rocking of BINAP with respect to the Ru(1)−Ru(2) edge, accompanied by the shift of the binaphthyl moiety to and from the metal framework in **A**,**B** and **C**, respectively. It seems very probable that the short contact of the hydride and binaphthyl proton in the **A**,**B** conformer discussed above can be considered as "dihydrogen bonding",[34−37] which compensates fpr the van der Waals repulsion of BINAP and other ligands to "organize" **2** into the **A**,**B** structure. This type of bonding is now recognized[34−37] as an important structural factor in transition-metal hydrides. Retention of these contacts in solution is well documented by the ^{1}H−^{1}H NOE measurements carried out for **2**. This is an important indication of the role this weak interaction may play in the determination of subtle structural features of the cluster hydrides.

Monitoring of the ^{1}H and ^{31}P NMR spectra in the temperature range 300−350 K in d_8-toluene showed substantial decomposition of the sample, which prevented a detailed characterization of the intramolecular dynamic processes that occur in **2** above 300 K. How-

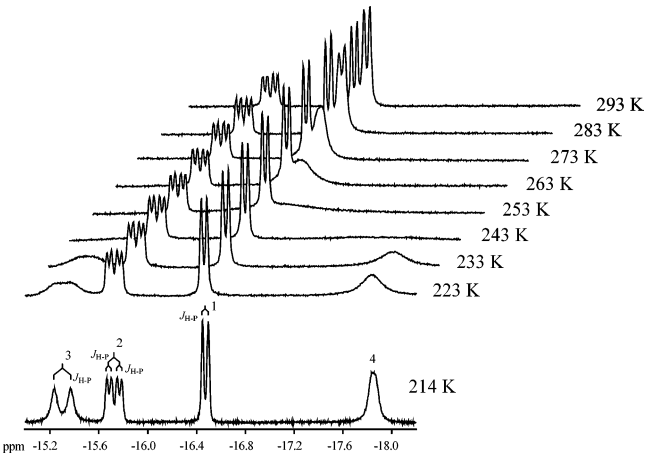

Figure 6. ^{1}H NMR spectrum of **3** in the hydride region (in $CDCl_3$, 214 K). The assignment of the hydride resonances is schematically shown at the top of the spectrum.

ever, extrapolation of the trends observed at lower temperatures most likely points to (a) complete scrambling of the hydride environment over the tetraruthenium skeleton and (b) oscillation of the BINAP binaphthyl system from one ruthenium triangle to another, to give the achiral "$H_4Ru_4(\mu$-PP)" pattern, as has been suggested earlier for other $H_4Ru_4(CO)_{12}$ derivatives containing asymmetric diphosphines.[22,40]

Cluster 3. The ^{1}H NMR spectrum of **3** features stereochemical nonrigidity of the hydride ligands above 200 K (Figure 6). In the limiting low-temperature spectrum shown in Figure 6, four well-resolved hydride resonances are observed between −15 and −18 ppm that points, similarly to **2**, to an asymmetric structure of the "$H_4Ru_4(\mu$-PP)" fragment. Selective $^1H\{^1H\}$, $^1H\{^{31}P\}$, and $^{31}P\{^1H\}$ decoupling measurements revealed the spin−spin coupling pattern shown in Chart 1. This allowed complete assignment of the proton NMR spectrum in the hydride region, which is shown at the top of Figure 6. The coupling diagram is essentially the same as that found for **2**, which testifies in favor of essentially similar locations of the hydrides around the tetraruthenium framework. This diagram also confirms the structure of the hydride environment suggested for **3** on the basis of X-ray crystallographic analysis. In agreement with this structure, the ^{31}P NMR spectrum also displays two doublets at 50.29 and 28.18 ppm (^3J(P−P) = 2.8 Hz). The highest value of ^2J(P−H) observed for H(03) and P(2) testifies in favor of their trans position around Ru(2), and asymmetric coupling of H(02) with the phosphorus nuclei (25.6 and 10.9 Hz) most likely points to the semibridging location of this hydride over the Ru(1)−Ru(2) edge.

Completely analogous to **2**, the ^{1}H NOE measurements for **3** ($CDCl_3$, 215 K, Figure S7) were very indicative in elucidation of the cluster molecular structure in solution. The short nonbonding contacts H(04)−H(13) (2.02 Å), H(01)−H(42) (2.44 Å), and H(02)−H(48) (2.19 Å) result in enhancement of the corresponding signals in the aromatic area upon selective irradiation of associated hydrides, whereas H(03) did not give a NOE response in the aromatic region because of its remote location with respect to the naphthyl fragments and phenyl rings of BINAP. Thus, irradiation into the H(04) frequency gives strong enhancement of the H(13) naphthyl proton signal (6.4 ppm), together with a weak response of H(14), whereas irradiation of H(01) and H(02) generates NOE responses related to H(42) (6.42 ppm) and H(48) (7.5 ppm) phenyl protons, respectively. It is relevant to note that the H(13) signal in **3** (dd due to H−H and P−H couplings) is substantially upfield shifted (6.4 ppm) compared to the signal of the same proton in **2** (dd, 7.8 ppm). This observation is completely in line with a regular high-field shift of the proton signals of coordinated double bonds and aromatic rings and suggests that coordination of the naphthyl fragment is maintained in solution.

Variable-temperature ^{1}H NMR measurements (Figure 6) showed essentially different dynamic behavior of **3** compared to **2**. In the temperature range 195−300 K, the hydride signals corresponding to H(01) and H(02) do not display any broadening, whereas those of H(04) and H(03) successively broaden, degrade to the baseline, and eventually collapse into a doublet at −16.5 ppm (J(P−H) = 15 Hz). In contrast to the hydride dynamics observed in **2**, where the scrambling process starts at 255 K and makes them all equivalent above 300 K, the H(04)−H(03) pairwise exchange in **3** starts at substantially lower temperature and does not involve two other hydrides in the whole temperature range studied. A plausible explanation of the early onset of the H(04) ↔ H(03) exchange observed in **3** may be derived from the changes in the H(04) coordination geometry caused by a ligand interaction with the adjacent naphthyl fragment. This interaction results in a shift of the bridging ligand away from the Ru(1)Ru(2)Ru(3) triangle (see Figure 2 and Table 2). One of the possible mechanisms of two μ_2-bridging ligand exchange is a **(**μ_2,μ_2**)** ↔ **(**μ_3,**t)** ↔ **(**μ_2,μ_2**)** sequence with a transition state including face-bridging and terminal hydrides. The shift of H(04) mentioned above brings it into close proximity to the position it has to occupy in the μ_3 transition state over the Ru(2)Ru(3)Ru(4) triangle, thus lowering the potential barrier of the exchange. It has to be stressed that H(03) ↔ H(04) exchange does not wipe out the asymmetry of the "H_4Ru_4(PP)" fragment. The VT ^{31}P NMR measurements showed two fairly narrow doublets corresponding to the strongly inequivalent phosphorus atoms of BINAP in the temperature range 190−343 K (Figure S8), which confirms that the cluster framework retains its chiral configuration despite the H(03) ↔ H(04) exchange. In contrast to **2**, no broadening of the ^{31}P signals was observed above 300 K; moreover, no decomposition of the sample was detected during the NMR experiments.

Thus, the NMR study of the cluster **3** clearly demonstrates its high stability in the temperature range covering possible conditions of hydrogenation catalysis. The data obtained prove that the asymmetric structure of this cluster revealed in the solid state remains unchanged in solution and the dynamics of the hydride ligands does not erase the chemical difference between the four ruthenium atoms of the cluster framework. Circular dichroism (CD) measurements discussed below reinforce this observation and confirm that the molecule bears chirality not only in the BINAP binaphthyl system but also in the asymmetric cluster core.

Stereochemistry of 2 and 3. The metal framework in tetrahedral clusters is a potentially chiral structural

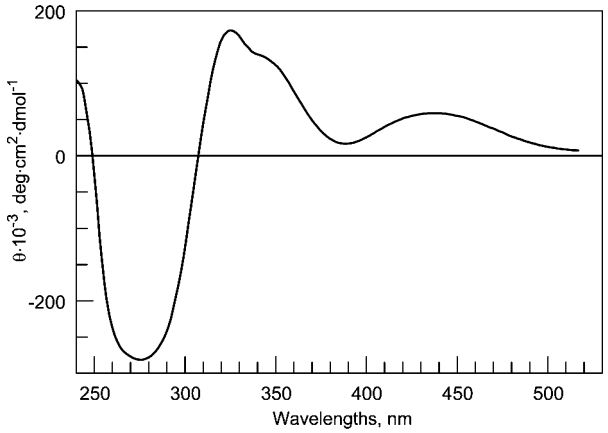

Figure 7. Circular dichroism spectrum of **3** (25 °C, in dichloromethane).

unit, the asymmetry of which emerges from the difference in chemical nature of the tetrahedron vertexes. Directed design of the differences in metal atom ligand environments is a way to induce chirality into a homonuclear M_4 cluster framework. The potential of a chiral molecule to act as an asymmetric catalyst depends strongly on its stereochemical stability, which is determined by the potential barrier for racemization processes. It has been shown earlier[46,47] that stereopure heteronuclear tetrahedral clusters easily racemize under catalytic conditions to give an effective but nondiscriminating catalyst. As a rule, the stability of configuration of the chiral ligands is substantially higher than that of the cluster framework, which results in predominant use of the "chiral-in-ligand" cluster catalysts where stereoinduction is dictated by the ligand asymmetry only.[14,22−25] Nevertheless, it is quite evident that a combination of the stereoinduction from the chiral ligand and from a stable asymmetric metal framework may give rise to enhanced stereoresolution of the catalyst, which was one of the driving forces for the present synthetic project.

The solid-state structure of **3** (Figure 2) clearly shows asymmetry of the ruthenium tetrahedron, in which all ruthenium atoms are distinguished by the difference in their ligand environment. On the basis of CIP rules,[48] one can assign the *S* stereoconfiguration to the "Ru_4" framework, treating it as an analogue of a tetrahedral carbon atom. The combination of two chiral elements in **3** ((*S*)-BINAP and (*S*)-"Ru_4") gives the *S*,*S* configuration of the diastereomeric molecule. The NMR spectroscopic study of **3** indicated that this absolute configuration remains unchanged in solution and showed unusually high thermal stability of the chiral framework in a fairly wide temperature range.

The presence of the tetraruthenium framework in its stereopure configuration is also supported by the CD spectrum of **3**, shown in Figure 7. The spectrum exhibits optical activity in the interval 220−500 nm. Analysis of the literature data shows that mononuclear complexes containing BINAP and its derivatives[49,50] normally display a CD response at the wavelengths below 350 nm.

To the best of our knowledge, the only example of the Cotton effect at longer wavelengths was observed for the $[Pd(BINAP)H_2O]^{2+}$ complex,[51] where an optical rotation band appears at about 400 nm. This makes it possible to assign the 220−400 nm features observed in the CD spectrum of **3** to binaphthyl-related, intraligand $\pi-\pi^*$, and MLCT electronic transitions. Longer wavelength absorptions in the electronic spectra of the cluster compounds are normally attributed to metal core based transitions, and a broad positive band observed between 400 and 500 nm can be assigned to the asymmetry of the "Ru_4" stereogenic center. The CD spectra obtained for the "chiral-in-framework" diastereomers of the $(\mu\text{-H})Os_3(CO)_{10}(\mu\text{-XY})$ (XY = (*R*)-(4-(1-hydroxyethyl)-2-pyridinyl), (*S*)-3-(*N*-methyl-2-pyrrolidinyl)-2-pyridinyl)) clusters[7] have been interpreted in a similar way. The Cotton effects observed in the 230−500 nm range have been considered characteristic of the $M_3(\mu\text{-XY})$ framework asymmetry, because chiral organic auxiliaries do not display electronic transitions in this interval. In the case of these triosmium clusters nearly no "synthetic" stereoresolution was observed and separation of the diastereomers was achieved using HPLC. In contrast, **3**, as well as **2**, have been synthesized as unique diastereoisomers according to the NMR and CD data.

This unique situation is completely determined by specific features of the BINAP stereochemistry. The structural patterns given in Chart 2 clearly show that as soon as the (*S*)-BINAP forms a "PP" bridge over a ruthenium−ruthenium edge, there is only one way for the binaphthyl system to occupy a μ_3-bridging position, namely, to use its "left hand" (P(2)-bound naphthyl fragment) in this bonding. This particular mode of the BINAP face-bridging coordination also determines the asymmetry of the hydride ligand design around the ruthenium tetrahedron, which does not disappear even under fast regime exchange of H(03) and H0(4).

Cluster 2. In the structural pattern shown in Chart 2, the "$(CO)_{10}Ru_4$(BINAP)" fragment in **2** is not chiral because the two "$Ru(CO)_2P$" centers are not stereochemically different but only diastereotopic. The tetrahedron becomes chiral, due to the asymmetry of the hydride ligand coordination to afford the *S* configuration of the ruthenium tetrahedron in the solid state. Similarly to **3**, no evidence for the presence of another *R*,*S* diastereomer has been observed, either in the solid state or in solution. However, **2** is substantially less stereochemically rigid compared to **3**. As mentioned above, decomposition of **2** upon heating above 300 K prevents a detailed characterization of the high-temperature dynamics in this cluster. Nevertheless, it is possible (fast heating, fast acquisition) to observe total scrambling of all hydrides over the tetraruthenium skeleton. This process together with rocking of the diphosphine relative to the Ru(1)−Ru(2) edge eventually results in the onset of a symmetry plane onto the "H_4Ru_4(PP)" fragment to give degradation of both phosphorus resonances into the baseline above 350 K. The racemization dynamics of this

(46) Richter, F.; Vahrenkamp, H. *Chem. Ber.* **1982**, *115*, 3243.
(47) Vahrenkamp, H. *J. Organomet. Chem.* **1989**, *370*, 65.
(48) *Pure Appl. Chem.* **1976**, *45*, 11.
(49) Evans, O. R.; Manke, D. R.; Lin, W. *Chem. Mater.* **2002**, *14*, 3866.
(50) Mikami, K.; Yusa, Y.; Aikawa, K.; Hatano, M. *Chirality* **2003**, *15*, 105.
(51) Muller, C.; Whiteford, J. A.; Stang, P. J. *J. Am. Chem. Soc.* **1998**, *120*, 9827.

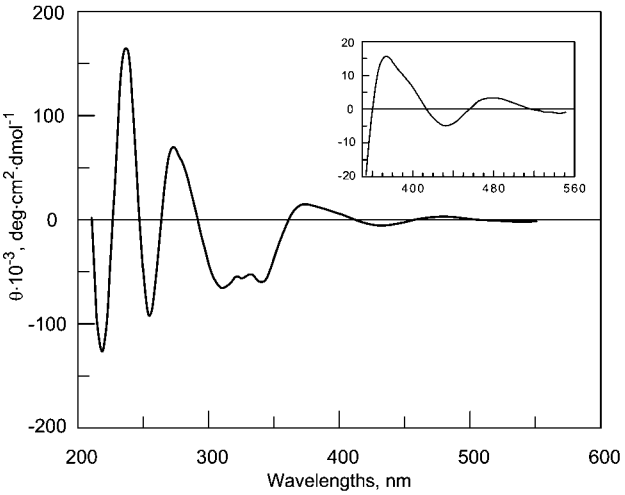

Figure 8. Circular dichroism spectrum of **2** (25 °C, in hexane).

sort may very likely account for the moderate chiral discrimination obtained with $H_4Ru_4(CO)_{12}$ derivatives containing asymmetric bridging diphosphines,[22] as compared to related mononuclear complexes. In the case of these tetranuclear ruthenium catalysts, which undergo metal framework racemization, the coordination and transformation of a substrate in a remote part of the molecule may be only slightly affected by the presence of the asymmetric diphosphine ligands.

Nevertheless, similar to the case for **3**, the room-temperature CD spectrum of **2** (Figure 8) displays optical activity in a relatively broad wavelength range. Positive and negative absorption bands in the 400−550 nm interval may be assigned to the "Ru_4" stereogenic center, which points to incomplete racemization of **2** at or below room temperature.

In conclusion, we have found the following.

1. The reaction of (*S*)-BINAP with $H_4Ru_4(CO)_{12}$ in the presence of trimethylamine *N*-oxide affords the substituted cluster $H_4Ru_4(CO)_{10}(\mu$-(*S*)-BINAP) (**2**), containing the diphosphine ligand coordinated in a bridging mode. Further gentle heating of **2** gives an unusual face-bridging coordination of BINAP in $H_4Ru_4(CO)_9(\mu_3$-(*S*)-BINAP) (**3**), additional bonding of the diphosphine occurring through the "double bonds" of the ligand naphthyl fragment. The structures of both clusters in the solid state have been established using X-ray crystallography. The solution structure of **2** and **3** and the dynamic behavior of the hydride ligands were elucidated using a wide range of NMR spectroscopic techniques.

2. The tetrahedral metal frameworks in **2** and **3** are chiral, due to the asymmetry of the ligand environment at each ruthenium atom. Syntheses of both clusters display extremely high *(100%)* stereoselectivity to give an *S*(BINAP),*S*(Ru_4) diastereoconfiguration of these molecules.

3. The cluster **3** demonstrates unusually high thermal stability, retaining stereoconfiguration of the metal framework intact up to 80 °C.

Final Remark. It has been discovered that **3** is not chemically inert. The cluster exhibits hemilability of the coordinated naphthyl fragment. Two-electron donors such as CO, acetonitrile, and 1-hexene can be easily added to **3** to restore the edge-bridging coordination of BINAP. The room-temperature reaction with CO immediately and quantitatively regenerates the starting $H_4Ru_4(CO)_{10}(\mu_2$-BINAP) cluster. The products of reactions with the other ligands mentioned above have been isolated, and the study of their structure and properties is now in progress. These results also point to the promising catalytic potential of **3**, which is now under investigation.

Acknowledgment. Financial support provided by the Russian Foundation for Basic Research (Grant 02-03-32792), the Nordic Council of Ministers (T.S.P. and S.P.T.), and the Academy of Finland (M.H.) is gratefully acknowledged. We thank Pavel Tsitovich for CD spectra recording and Drs. I. S. Podkorytov and P. S. Lobanov for fruitful discussions of related NMR and stereochemical problems.

Supporting Information Available: Tables giving crystallographic data and figures giving ^{1}H COSY, EXSY, and difference NOE NMR spectra of the clusters **2** and **3**; crystallographic data are also available as CIF files. This material is available free of charge via the Internet at http://pubs.acs.org.

OM034288N